Satellites of Xe transitions induced by infrared active vibrational modes of CF4 and C2F6 molecules

Vadim A. Alekseev and Nikolaus Schwentner

Citation: The Journal of Chemical Physics **135**, 044313 (2011); doi: 10.1063/1.3615160

View online: http://dx.doi.org/10.1063/1.3615160

View Table of Contents: http://scitation.aip.org/content/aip/journal/jcp/135/4?ver=pdfcov

Published by the AIP Publishing

Satellites of Xe transitions induced by infrared active vibrational modes of CF_4 and C_2F_6 molecules

Vadim A. Alekseev[1,a)] and Nikolaus Schwentner[2]
[1]*Institute of Physics, St.Petersburg State University, Ul'janovskaja St.1, Peterhof 198504, Russia*
[2]*Institut für Experimentalphysik, Freie Universität Berlin, Arnimallee 14, D-14195 Berlin, Germany*

(Received 21 April 2011; accepted 2 July 2011; published online 28 July 2011)

Absorption and luminescence excitation spectra of Xe/CF_4 mixtures were studied in the vacuum UV region at high resolution using tunable synchrotron radiation. Pressure-broadened resonance bands and bands associated with dipole-forbidden states of the Xe atom due to collision-induced breakdown of the optical selection rules are reported. The spectra display in addition numerous satellite bands corresponding to transitions to vibrationally excited states of a Xe-CF_4 collisional complex. These satellites are located at energies of Xe atom transition increased by one quantum energy in the IR active ν_3 vibrational mode of CF_4 ($\nu_3 = 1281$ cm^{-1}). Satellites of both resonance and dipole-forbidden transitions were observed. Satellites of low lying resonance states are spectrally broad bands closely resembling in shape their parent pressure-broadened resonance bands. In contrast, satellites of dipole-forbidden states and of high lying resonance states are spectrally narrow bands (FWHM ~10 cm^{-1}). The satellites of dipole-forbidden states are orders of magnitude stronger than transitions to their parent states due to collision-induced breakdown of the optical selection rules. These satellites are attributed to a coupling of dipole-forbidden and resonance states induced by the electric field of the transient CF_4 ($\nu_3 = 0 \leftrightarrow \nu_3 = 1$) dipole. Similar satellites are present in spectra of Xe/C_2F_6 mixtures where these bands are induced by the IR active ν_{10} mode of C_2F_6. Transitions to vibrationally excited states of Xe-CF_4(C_2F_6) collision pairs were also observed in two-photon LIF spectra. © *2011 American Institute of Physics*. [doi:10.1063/1.3615160]

I. INTRODUCTION

Vacuum (Vac) UV spectra of pure Xe gas and of mixtures with lighter rare gases (Rg) have been a subject of several studies (Refs. 1 and 2 and references therein). Spectra of pure Xe show extended quasimolecular absorption on the red wings of the resonance lines corresponding to transitions from the repulsive ground state of Xe–Xe pairs to strongly bound excited states of Xe_2^*. In contrast, the Xe–Rg′ interaction potentials correlating with the lowest Xe resonance states are strongly repulsive due to repulsion of the Rydberg electron from the closed shell Rg′ atom (Pauli repulsion). The pressure-broadened resonance bands in Xe/Rg′ mixtures are therefore degraded to the blue. Besides the transitions on the wings of resonance lines, spectra of Xe and Xe/Rg′ mixtures also show quasimolecular transitions correlating with dipole-forbidden states of the Xe atom.

In comparison to other molecular gases, perfluoromethan has peculiar properties which support the observation of collision-induced transitions in absorption and luminescence excitation spectra of Rg/CF_4 mixtures (Rg = Xe, Kr). This gas is transparent in the Vac UV region up to λ ~115 nm. Furthermore, collisions with CF_4 do not deactivate high lying excited states of the Xe and Kr atoms but efficiently transfer populaton to the lowest Xe $6s[3/2]_2$ and Kr $5s[5/2]_2$ metastable states. The metastable atoms decay following thermal activation to the resonance states lying ~1000 cm^{-1} higher in energy.

Early studies of Xe/CF_4 and Kr/CF_4 mixtures in the Vac UV region revealed strong quasimolecular absorption on the blue wings of Rg $ns[3/2]_1$ resonance lines and satellite transitions shifted ~1000 cm^{-1} further to the blue (Ref. 3 and references therein). In comparison to mixtures with light rare gases,[1,2] blue wing absorption in mixtures with CF_4 covers a broader spectral region implying stronger repulsion between excited atom and molecule. The early studies [3] were conducted with low spectral resolution. Recently, Xe/CF_4 and Kr/CF_4 was studied at high spectral resolution including the $\lambda < 120$ nm region which was omitted in Ref. 3 due to low intensity of the discharge light source. The high resolution data proved the assignment of satellites of resonance transitions (SRs) to vibrationally excited state of the collisional complex.[4] The SRs are shifted from their parent resonance transitions by one quantum energy of the IR active ν_3-mode of CF_4. The corresponding photoprocess may be written as follows:

$$\mathrm{Xe}(G) + \mathrm{CF_4}\ (\nu_3 = 0) + h\nu \rightarrow \mathrm{Xe}(R) + \mathrm{CF_4}\ (\nu_3 = 1), \tag{1}$$

where G and R denote the ground and a resonance states, respectively. Furthermore, the high resolution studies revealed numerous spectrally narrow satellites of dipole-forbidden transitions (SDFs) in the Xe atom.[5] These satellites are also

a)Author to whom correspondence should be addressed. Electronic mail: alekseev@va3474.spb.edu.

induced by the ν_3-mode and correspond to

$$\mathrm{Xe}(G) + \mathrm{CF_4}\ (\nu_3 = 0) + h\nu \rightarrow \mathrm{Xe}(DF) + \mathrm{CF_4}\ (\nu_3 = 1) \tag{2}$$

photoprocess, where DF denotes a dipole-forbidden state which cannot be accessed optically from the ground state.

Although processes (1) and (2) are formally similar, the mechanisms for borrowing transition strength are different for SR and SDF. The following conclusions concerning the differences between SR and SDF have been derived:[5]

(i) SR are spectrally broad bands closely resembling in shape their parent pressure-broadened resonance bands. It implies that SRs correspond to transitions at small distances between atom and molecule, where Xe(G)–CF_4 ($\nu_3 = 0$) and Xe(R)–CF_4 ($\nu_3 = 1$) interaction potentials are not parallel. In contrast, spectrally narrow SDF bands (FWHM $\sim$10 $\mathrm{cm^{-1}}$) closely match the asymptotic energies of the Xe(DF) + CF_4 ($\nu_3 = 1$) collisional pair implying transitions at large distances, where Xe(G)–CF_4 ($\nu_3 = 0$) and Xe(DF)–CF_4 ($\nu_3 = 1$) interaction potentials are nearly parallel.

(ii) SDF are much more intense in comparison to SR. The absorption cross section for the most intense SDFs reaches 10^{-35} $\mathrm{cm^5}$, and therefore, these bands are already seen in mixtures containing only few mbar of Xe and CF_4. The SR absorption cross section for comparison is $\sim 10^{-38}$ $\mathrm{cm^5}$.

Intense SDFs are usually observed on the wings of pressure-broadened resonance transitions.[5] These bands are especially strong when Xe($R \leftrightarrow DF$) is a dipole allowed transition. This effect may be explained by an intensity borrowing from the resonance transition,

$$\mathrm{Xe}(G) + \mathrm{CF_4}\ (\nu_3 = 0) + h\nu \rightarrow \mathrm{Xe}(R) + \mathrm{CF_4}\ (\nu_3 = 0), \tag{3}$$

induced by interaction of Xe($R \leftrightarrow DF$) and CF_4 ($\nu_3 = 0 \leftrightarrow \nu_3 = 1$) transient dipoles. The dipole–dipole interaction matrix element is given by

$$\alpha = \langle \Psi_{DF} | \mathrm{U_{dd}} | \Psi_R \rangle = \mu_{R \leftrightarrow DF} \mu_{\nu 3}\ \Phi / R^3,$$

where $\Psi_{DF} = \psi_{\mathrm{Xe}}(DF)\psi_{\mathrm{CF4}}(\nu_3 = 1)$ and $\Psi_R = \psi_{\mathrm{Xe}}(R)\psi_{\mathrm{CF4}}(\nu_3 = 0)$ are wavefunctions of dipole-forbidden and resonance states written as products of atomic and molecular wavefunctions, $\mu_{R \leftrightarrow DF}$ and $\mu_{\nu 3}$ are the dipole moments of atomic and molecular transitions, Φ is a factor depending on the angular orientation of the instantaneous dipoles, and R is the distance between atom and molecule. The upper state wavefunction of Eq. (2) may be written as $c_{DF}\Psi_{DF} + c_R\Psi_R$. For a large R when $\alpha \ll \Delta$, we have $c_{DF} \sim 1$ and $c_R \sim \alpha / \Delta$, where Δ is the energy gap between Xe(DF) + CF_4 ($\nu_3 = 1$) and Xe(R) + CF_4 ($\nu_3 = 0$) states. The dipole moment of Eq. (2) is given by

$$\mu_{G \leftrightarrow SDF} = \langle c_{DF}\ \Psi_{DF} + c_R \Psi_R | \mu_{G \leftrightarrow R} | \Psi_G K \rangle \sim (\alpha / \Delta) \mu_{G \leftrightarrow R},$$

where $\Psi_{\mathrm{GS}} = \psi_{\mathrm{Xe}}(G)\psi_{\mathrm{CF4}}(\nu_3 = 0)$, and $\mu_{G \leftrightarrow R}$ is the dipole moment of the resonance transition. If the difference in energies of Eqs. (2) and (3) is neglected, the SDF absorption cross sections are given by

$$\sigma_{\mathrm{SDF}} \approx (\alpha / \Delta)^2 \sigma_R, \tag{4}$$

where σ_R is the atomic resonance absorption cross section. For strong resonances, $\sigma_R \sim 10^4$ Å^2 and SDF are readily seen when $(\alpha/\Delta)^2$ is only $\sim 10^{-4}$.

Similar satellites due to IR active modes of molecules may be observed in spectra of other atomic gas–molecular gas mixtures. Studies of Xe/C_2F_6 mixtures revealed satellites due to IR active ν_{10} -mode of C_2F_6.[5] Like the ν_3-mode of CF_4, this mode is related to stretch of the C–F bond. The energy difference ν_3 (CF_4)–ν_{10}(C_2F_6) is only 30 $\mathrm{cm^{-1}}$ and the corresponding energy shift in positions of spectrally narrow SDF bands is clearly seen in high resolution spectra.[5] An accidental proximity of atomic $R \leftrightarrow DF$ and IR active vibrational transitions may be found for many atom molecule pairs. In particular, the Na ($3p_{3/2,1/2} \leftrightarrow 3d_{5/2,3/2}$) and CF_4 ($\nu_3 = 0 \leftrightarrow \nu_3 = 1$) transition energies differ by 180 $\mathrm{cm^{-1}}$. It has been demonstrated that the

$$\mathrm{Na}(3s) + \mathrm{CF_4}(\nu_3 = 0) + h\nu \rightarrow \mathrm{Na}(3d) + \mathrm{CF_4}\ (\nu_3 = 1)$$

process is readily observed in LIF spectrum of Na/CF_4 mixture in a static cell.[6] Simultaneous optical excitation of Na and CF_4 has been studied in further details in a crossed beam experiment.[7] Excited Na atoms were preferably found at small scattering angles implying excitation at large impact parameter which is consistent with the long-range character of the dipole–dipole interaction.

Processes in which absorption or emission of one photon changes quantum states of two particles are known from studies of other binary systems. Excitation of two ground states atoms,

$$\mathrm{A}(G) + \mathrm{B}(G) + h\nu \rightarrow \mathrm{A}(DF) + \mathrm{B}(R),$$

has been observed in spectra of mixtures of IA–IIIA group metals (Cs, Rb, Cs-Rb, Ba, Ba-Tl).[8,9] Collisions of a ground state atom with an optically excited resonance state atom

$$\mathrm{A}(G) + \mathrm{B}(R) + h\nu \rightarrow \mathrm{A}(DF) + \mathrm{B}(G)$$

(radiative collisions,[10] laser induced collisional energy transfer [11]) have been studied as well. Simultaneous vibrational excitation of two molecules has been observed in high pressure mixtures of molecular gases, cryogenic liquids, and molecular layers adsorbed on a surface (Refs. 12 and 13 and references therein). Vibrational satellites of atomic transitions have been reported in absorption and luminescence spectra of atom doped molecular solids.[14–16]

Our previous paper on vibrationally induced transitions in Vac UV spectra of Xe/CF_4 mixtures[5] was focused on a narrow 88 000–90 500 $\mathrm{cm^{-1}}$ range around the Xe $6d[3/2]_1$ resonance. In the present paper, we investigate vibrational satellites in further detail. The above conclusions on the origin of satellite bands are verified for a large manifold of Xe transitions in a broad range from 68 000 $\mathrm{cm^{-1}}$ (the first Xe resonance line) up to 95 000 $\mathrm{cm^{-1}}$ (the LiF window cutoff). The Xe atom energy level diagram in Fig. 1 serves as a guide through the complex spectra (the range around Xe $6d[3/2]_1$ is omitted). In Sec. III A, we present results on SR in the region of the Xe $6s$, $6s'$, and $7s$ resonance states (left-hand side of Fig. 1) and discuss spectral similarities of the Xe $6s[3/2]_1$

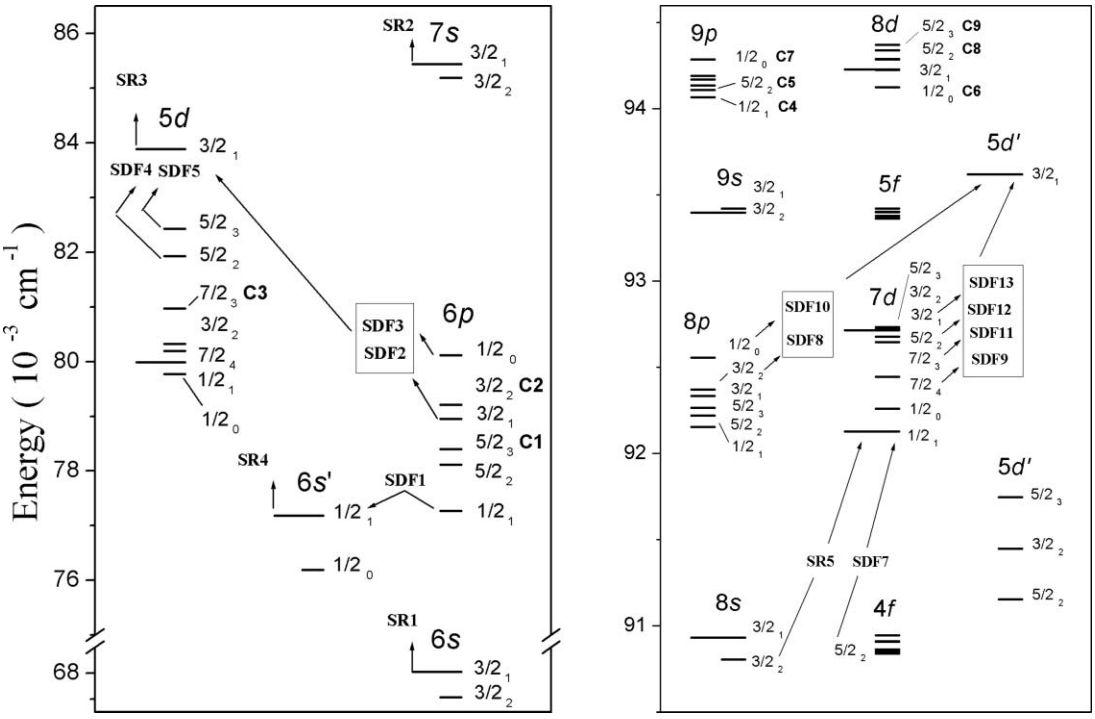

FIG. 1. The Xe atom energy levels diagram (Ref. 17) in the jl-coupling notation, nl[K]$_J$, where K = j($5p^5$) + l(nl) and J = K + 1/2; the j($5p^5$) = 1/2 ion-core states have index prime. The 86 000–90 000 region is omitted. Resonance states are shown by longer lines. Observed transitions to dipole-forbidden states due to collision-induced breakdown of optical selection rules are labeled C1–C9. Observed satellites of resonance transitions are shown by vertical arrows and labeled SR1–SR5. Satellites of dipole-forbidden transitions are shown by arrows pointing toward the enhancing resonance state and labeled SDF1–SDF13.

SR and the Kr $5s[3/2]_1$ SR. Then, we go up consecutively in energy starting with the Xe $5d[1/2]_1$ resonance region in Sec. III B. Besides SR and SDF, the spectra in this region also show intense quasimolecular bands related to dipole-forbidden states of the Xe atom. The upper states of these transitions correlate with Xe(DF) + CF_4 ($\nu_3 = 0$). Their parent states are labeled C1–C9 in Fig. 1. In Sec. III C, we discuss the spectrum near the strong Xe $5d[3/2]_1$ resonance (left-hand side of Fig. 1). The region of high lying Xe 8s, 7d, 5d', and 8d states (right-hand side of Fig. 1) is considered in Sec. III D. The abbreviations in Fig. 1 are used in all figures and in the text. Section III E concerns with studies of Xe/C_2F_6 mixtures. Finally, in Sec. III F, we discuss two-photon LIF spectra of Xe/CF_4 and Xe/ C_2F_6 mixtures and show an example of a vibrational satellite of the Xe $6p[1/2]_0$ two-photon resonance state.

II. EXPERIMENTAL

The experiments were conducted at the synchrotron radiation facility BESSY using a 10-m normal incidence monochromator.[18] The cell was constructed from a standard CF65 cross-shape vacuum connector (Leybold) and was separated from the high vacuum part of the experimental setup by LiF windows. Rare gases and CF_4 (Linde) were used without further purification. Transmitted light was detected by a GaAs photodiode or by a photomultiplier tube (PMT) installed behind a screen covered with sodium salicylate luminophore. Absorption spectra of pure Xe and Kr at low pressure (<1 mbar) were used for the absolute wavelength calibration. The accuracy is ~0.5 cm^{-1}. The absorption cross section (σ) of Xe-CF_4 collisional pairs was derived from the intensity (I), the cell length (L), and the partial pressures according to the Lambert-Beer law,

$$I = I_0 \exp(-\sigma\ L\ [Xe][CF_4]).$$

Undispersed emission of Rg/CF_4 mixtures excited by SR radiation was detected via side-on windows. One window was made of MgF_2 to observe emission in the Vac UV range with use of a solar blind photomultiplier, which is sensitive in the 114–350 nm region. Emission in the UV and visible spectral ranges was recorded via the second on-side window with the use of another photomultiplier.

Side-on photomultipliers accept luminescence excited in the spatial region near the cell center. When absorption is strong (for example, near the resonance wavelength), only a small fraction of SR flux reaches the cell center. To increase the luminescence intensity in the cell center, the entrance window was mounted close to the center with use of a special adapter attached to the entrance flange of the cell.

III. RESULTS AND DISCUSSION

A. Resonance n*s* and n*s*′ transitions of Xe and Kr atoms

Shapes of pressure-broadened Xe $6s[3/2]_1$ and Kr $5s[3/2]_1$ resonances in mixtures with CF_4 and C_2F_6 have been discussed in some details in Ref. 19. Figure 2(a) shows spectra of Xe (1) and Kr (2) in mixture with CF_4. In terms of spectral width and structural features (typically one or two shoulders), these spectra are similar. The red wing absorption covers ~50 cm^{-1} and is already seen at relatively small CF_4 pressures of

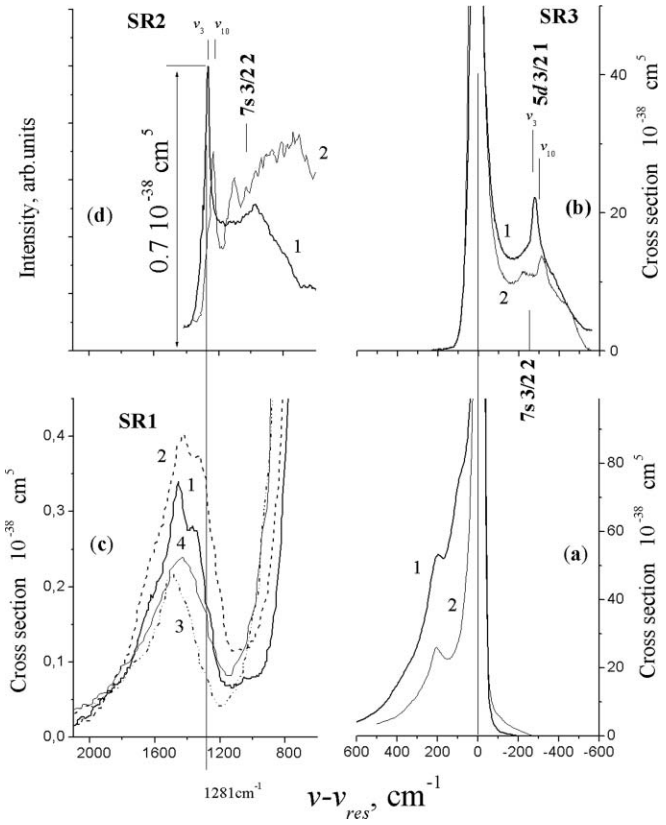

FIG. 2. (a) The Xe $6s[3/2]_1$ (1) and Kr $5s[3/2]_1$ (2) resonances in mixture with CF_4, (b) the Xe $7_s[3/2]1$ resonance in mixture with CF_4 (1) and c_2F_6 (2), (c) satellite of Xe $6_s[3/2]1$ (1) in mixture with CF_4, (d) satellite of Xe $7s[3/2]_1$ in luminescence excitation spectra of mixtures with CF_4 (1) and C_2F_6 (2). Panel (c) also shows satellite of Xe $6s[3/2]_1$ in mixture with C_2F_6 (2), and satellites of Kr $5s[3/2]_1$ in mixtures with CF_4 (3) and C_2F_6 (4). The lower sticks in (b) indicates the energy of Xe $7s[3/2]_2$ (relative to Xe $7s[3/2]_1$) and the upper sticks in (b) and (d) indicate energies of Xe $5d[3/2]_1$ and Xe $7s[3/2]_1$ increased by the vibrational quantum energy of ν_3-mode of CF_4 ($\nu_3 = 1281\ cm^{-1}$) and ν_{10}-mode of C_2F_6 ($\nu_{10} = 1251\ cm^{-1}$). Some spectra for this Figure are taken from Refs. 4 and 19. Reprinted with permission from AIP Conf. Proc. Copyright 2008 American Institute of Physics.

about 10 mbar. The absorption continuum on the blue wing appears at higher pressures and covers $\sim$500 cm^{-1} of spectral width.

Like Rg atoms, CF_4 possesses no positive electron affinity.[20] Thus, this blue wing broadening of the first Rg n$s[3/2]_1$ resonances is likely due to repulsion of the excited atomic Rydberg electron from the closed shell molecular system (Pauli repulsion). This type of interaction is known for heteronuclear Rg′–Rg dimers, where it results in maxima on Rg*–Rg′ potentials.[21] As noted in Sec. I, this blue wing broadening in mixture with CF_4 covers a broader spectral region in comparison with Rg′/Rg mixtures. The binding in CF_4 is strongly ionic. According to *ab initio* calculations, a charge which is approximately equivalent to the charge of one electron is transferred from the central carbon atom to fluorine atoms.[22] It is likely that the stronger repulsive interaction between Rg* and CF_4 in comparison with the Rg*–Rg′ case is due to this extra negative charge on the fluorine atoms around the carbon core.

Due to the delocalization of the Rydberg electron density, the Pauli repulsion decreases with increase of the principal quantum number and the interaction potential becomes attractive owing to attraction to the ion core. Spectra of Xe $6s[3/2]_1$ and Xe $7s[3/2]_1$ in Figs. 2(a) and 2(b) nicely illustrate this tendency. As is seen, the increase of principal quantum number by one changes the interaction from repulsive for Xe $6s[3/2]_1$ to attractive for Xe $7s[3/2]_1$ with an inverted wing structure. A similar effect is observed for the Xe n*d* resonance states discussed in Sec. III C.

Spectra of pressure-broadened resonances were recorded at a Xe pressure $\sim$1 mbar and few hundred mbar of CF_4. Observation of SRs corresponding to process (1) requires a higher Xe partial pressure, typically $\sim$10–50 mbar. An absorption spectrum for the Xe $6s[3/2]_1$ satellite is shown in Fig. 2(c) (spectrum 1). The Xe $7s[3/2]_1$ SR (SR2) in a luminescence excitation spectrum is displayed in Fig. 2(d) (spectrum 1, absorption scale is indicated by the vertical arrow). The CF_4 gas is transparent in this spectral region and absorption and luminescence excitation spectra are nearly identical in shape.

As can be seen from Fig. 2, the SRs resemble their parent bands in shape. The shift between the red wings of the Xe $6s[3/2]_1$ resonance band and its satellite and the shift between the blue wings of the Xe $7s[3/2]_1$ resonance band and its satellite closely match the energy of the CF_4 vibrational quantum $\nu_3 = 1281\ cm^{-1}$. For the Xe $6s[3/2]_1$ state, the interaction potential is repulsive, and following optical excitation, the collisional complex dissociates yielding a resonance state atom and a vibrationally excited molecule. In contrast, transitions on the red wing of the Xe $7s[3/2]_1$ resonance or its satellite terminate at bound states. The width of these bands shows that the binding energy is at least $\sim$500 cm^{-1} or larger considering that for collisions at room temperature energies, only a part of the upper bound potential is optically accessible from the repulsive ground state.

Luminescence excitation spectra of Xe/CF_4 mixtures are similar in shape to the absorption spectra. There is no noticeable change in the luminescence quantum yield of a Xe/CF_4 mixture when the wavelength is tuned across the red wing of the Xe $7s[3/2]_1$ resonance or its SR. It implies that the process,

$$Xe(7s[3/2]1)..CF_4 \rightarrow Xe(^1S_0) + CF_3 + F,$$

does not take place, although the excitation energy is well above the CF_3–F bond dissociation energy (5.6 eV). The $Xe(7s[3/2]_1)..CF_4$ bound complex likely decays either spontaneously (predissociation or radiative decay) or in collisions with CF_4 yielding lower lying excited states of the Xe atom.

The Xe $7s[3/2]_1$ SR may have contributions from two different coupling mechanisms. The sharp blue feature (Fig. 2(d)) matching the asymptotic energy of Xe $7s[3/2]_1 + CF_4$ ($\nu_3 = 1$) collision pair may be due to the long range coupling mechanism with the very strong Xe $5d[3/2]_1$ resonance (see transition strengths in Table I) via intermediate Xe n*p* states. As shown in Secs. III B and III C, coupling with this resonance results in several other spectrally narrow satellites. In turn, the broad band shifted to the red from the asymptotic energy (Fig. 2(d)) may be due to the short range coupling mechanism similar to that which is responsible for the spectrally broad satellite of the Xe $6s[3/2]_1$ resonance (Fig. 2(c), spectrum 1).

TABLE I. Strengths of some transitions in the Xe atom (Ref. 23).

	S (a.u.)/transition energy (cm^{-1})				
	$6s'[1/2]_1$	$5d[1/2]_1$	$5d[3/2]_1$	$7s[3/2]_1$	$7s[3/2]_2$
$5p^6$	1.31	0.03	4.29	0.21	
$6p[1/2]_1$	12.9	20.6	0.2	1.47	22.5
$6p[5/2]_2$	0.01	1.74	2.34	31.5	16.2
$6p[3/2]_1$	0.57	0.57	30.4	31.2	2.45
$6p[3/2]_2$	6.56	5.23	0.09	19.9	43.6
$6p[1/2]_0$	1.86	0.77	35.2	16.1	

Table I lists strengths of some transitions in the Xe atom. As can be seen, the transitions from Xe $6p[3/2]_1$ and Xe $6p[1/2]_0$ to both the Xe $5d[3/2]_1$ and Xe $7s[3/2]_1$ resonance states have rather large strengths and these states may act as intermediate in the long range coupling mechanism. For the Xe $7s[3/2]_2$ state, there are no coupling routes of comparable strength and this may explain the absence of a Xe $7s[3/2]_2$ satellite (Fig. 2(d)). A case when both Xe n*s* states have satellites is discussed in Sec. III D.

Along with the Xe $6s[3/2]_1$ SR in mixture with CF_4, Fig. 2(c) also shows, for comparison, the satellite of this resonance in mixture with C_2F_6 as well as satellites of the Kr $5s[3/2]_1$ resonance in both mixtures. As can be seen, these bands have very similar blue graded shapes. The Kr $5s[3/2]_1$ resonance (S = 0.718 a.u. (Ref. 23)) is a factor of 1.3 weaker than Xe $6s[3/2]_1$. Satellite intensities correlate with transition strengths. The Kr $5s[3/2]_1$ SR in both CF_4 and C_2F_6 mixtures is ~1.5 times weaker than the Xe $6s[3/2]_1$ SR. Intensities also correlate with the intensities of vibrational transitions. The CF_4 ($\nu_3 = 0 \rightarrow \nu_3 = 1$) and C_2F_6 ($\nu_{10} = 0 \rightarrow \nu_{10} = 1$) transitions were calculated using the NIST Computational Chemistry Comparison and Benchmark Database.[24] The intensity ratio of ν_{10} to ν_3 was ~1.3 for all tested basis sets. The intensity ratio of SR in C_2F_6 to SR in CF_4 is close to this value (Fig. 2(c)). The Kr $5s'[1/2]_1$ SR in mixture with CF_4 was also observed. This band is nearly identical in shape and intensity to the Kr $5s[3/2]_1$ SR, as shown in Fig. 2(c) (spectrum 3). It should be noted in this respect that strengths of Kr $5s'[1/2]_1$ (S = 0.678 a.u. (Ref. 23)) and Kr $5s[3/2]_1$ (see above) are also nearly equal. Satellite of the corresponding Xe $6s'[1/2]_1$ resonance is spectrally overlapped with other transitions in the Xe spectrum (see below).

The C_2F_6 molecules strongly absorb Vac UV radiation in the $\lambda < 120$ nm region which complicates studies (this was an obstacle for recording the Kr $5s'[1/2]_1$ SR). On the other hand, collisions with C_2F_6 do not nonradiatively quench high lying Xe atom states but transfer population to the Xe 6*s* states, which decay radiatively. Therefore, some satellites of high lying states may still be seen in luminescence excitation spectra. Figure 2(d) shows Xe $7s[3/2]_1$ SR in a luminescence excitation spectrum. Like in mixture with CF_4, this band has a sharp blue wing and the small shift due to the difference of ~30 cm^{-1} in ν_3 and ν_{10} vibrational quanta is clearly seen. The onset of C_2F_6 absorption coincides spectrally with Xe $7s[3/2]_1$ SR. The C_2F_6 absorption cross section in this region significantly increases as wavelength decreases, and as a result, the luminescence intensity on the blue wing of this satellite is partially suppressed by stronger absorption.

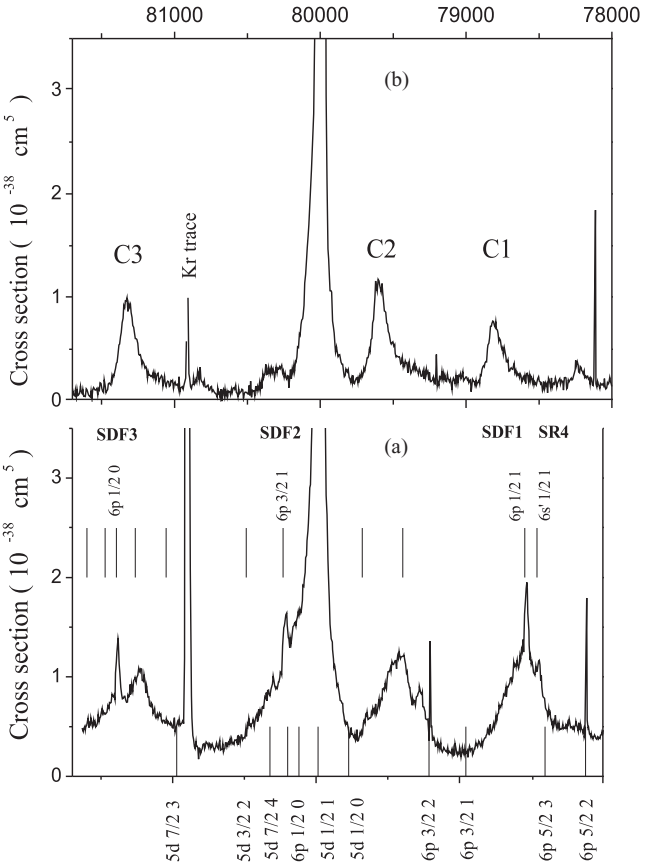

FIG. 3. Absorption cross section in the region of the Xe $5d[1/2]_1$ resonance. Mixtures: Xe 5 mbar/CF_4 800 mbar (a) and Xe 4 mbar/He 940 mbar (b). The lower sticks indicate the Xe atom level energies and the upper sticks indicate ν_3 satellites energies.

In conclusion of this section, we note that no satellite bands due to excitation of other vibrational modes of CF_4 and C_2F_6 were found in the present study. Hot bands originating from vibrationally excited Xe(*G*) + CF_4 ($\nu_3 = 1$) collision pairs were not observed as well. Experiments at elevated temperature might reveal such bands.

B. Xe $5d[1/2]_1$ resonance state

The Xe $5d[1/2]_1$ resonance is relatively weak and a higher partial pressure of Xe (typically few mbar) is needed to obtain a strong pressure-broadened band. Spectra of mixtures with CF_4 and He in the Xe $5d[1/2]_1$ region are compared in Fig. 3. In mixture with CF_4 (Fig. 3(a)), the broadening effect is more pronounced on both wings of the Xe $5d[1/2]_1$ resonance (absorption on the red wing in mixture with He is mainly due to Xe_2). The spectrum with He (Fig. 3(b)) displays several transitions to electronic states correlating with Xe(*DF*) states. The three most intense bands are labeled C1–C3. Similar red shaded bands have been observed in mixtures with Ne and Ar.[1,2] Accepting the assignment suggested in Ref. 1, one finds that these bands are shifted by ~400 cm^{-1} to the blue from their parent dipole-forbidden transitions. In the heavier Rg gases, the shift is smaller.[1]

The spectrum with CF_4 (Fig. 3(a)) displays three similar collision-induced bands which are spectrally broader and less shifted to the blue in comparison with Rg gases. Transitions to vibrationally excited states of Xe–CF_4 complex need to be considered as well. As seen from Fig. 3(a), the band C1 is spectrally overlapped with the Xe $6s'[1/2]_1$ satellite (SR4). Similar to the Xe $6s[3/2]_1$ resonance (Fig. 2(a)), the Xe $6s'[1/2]_1$ resonance in mixture with CF_4 is blue shaded (spectrum not shown) and, thus, the Xe $6s'[1/2]_1$ SR is expected to be blue shaded and overlapped with band C1. The Xe $6s'[1/2]_1$ SR is, however, too weak to resolve the shape, which is consistent with the following consideration. The Kr $5s[3/2]_1$ and Kr $5s'[1/2]_1$ resonances have nearly equal strengths and the intensities of their SRs are nearly the same (see Sec. III A). The Xe $6s[3/2]_1$ and Xe $6s'[1/2]_1$ resonances also have comparable strengths (S = 1.36 and 1.31 a.u. (Ref. 23)) and the same is expected for their SRs. Absorption cross sections for the Xe 6s$[3/2]_1$ SR and band C1 differ by a factor of 4 (compare band C1 in Fig. 3(a) with spectrum (1) in Fig. 2(c)) and, thus, the Xe $6s'[1/2]_1$ SR is likely by a factor of 4 weaker than band C1.

The spectrum in Fig. 3(a) displays in addition several spectrally narrow bands which may be unambiguously assigned as satellites of dipole-forbidden transitions. The sharp SDF1 band on the top of band C1 is satellite of Xe $6p[1/2]_1$. The Xe $(6p[1/2]_1 \leftrightarrow 6s'[1/2]_1)$ transition is strong (Table I) and SDF1 most likely borrows transition strength from the Xe $6s'[1/2]_1$ resonance owing to mixing with the Xe $6s'[1/2]_1 + CF_4$ $(\nu_3 = 0)$ resonance state induced by interaction of transient dipoles (see Sec. I).

The other two narrow bands in Fig. 3(a) labeled SDF2 and SDF3 are satellites of Xe $6p[3/2]_1$ and Xe $6p[1/2]_0$, respectively. These transitions likely borrow strength from the Xe $5d[3/2]_1$ resonance. As can be seen from Table I, both the Xe $(6p[3/2]_1, 6p[1/2]_0 \leftrightarrow 5d[3/2]_1)$ transitions are strong. In turn, the weakness of Xe $(6p[3/2]_2, 6p[5/2]_2 \leftrightarrow 5d[3/2]_1)$ transitions explains the absence of the corresponding SDFs. The Xe $5d[1/2]_1$ resonance is very weak and cannot be a source of transition strength neither for own SR nor for Xe $6p$ SDFs

C. Xe $5d[3/2]_1$ resonance state

Figure 4 shows some spectra in the region of the Xe $5d[3/2]_1$ resonance. The resonance band itself is blue shaded (spectrum 1) implying a repulsive interaction with CF_4. In contrast, the Xe $6d[3/2]_1$ band is red shaded [5] and, thus, similar to the Xe $6s/7s$ pair (Fig. 2(a) and 2(b)), an increase of the principal quantum number by one changes the interaction from repulsive to attractive.

The sharp SDF4 and SDF5 bands in Fig. 4 are unambiguously assigned as ν_3 satellites of Xe $5d[5/2]_2$ and Xe $5d[5/2]_3$. For comparison, Fig. 4 shows the spectrum of a mixture with C_2F_6. The shift in SF5 corresponding to the energy difference $\Delta = \nu_3\ (CF_4) - \nu_{10}(C_2F_6) = 30\ cm^{-1}$ is clearly seen. In contrast to Xe $6p$ SDFs discussed in Sec. III B, the Xe $5d$ SDFs are a second order effect of electric field induced mixing between forbidden and resonance states with the Xe np states acting as intermediate. No such SDFs are seen in the region

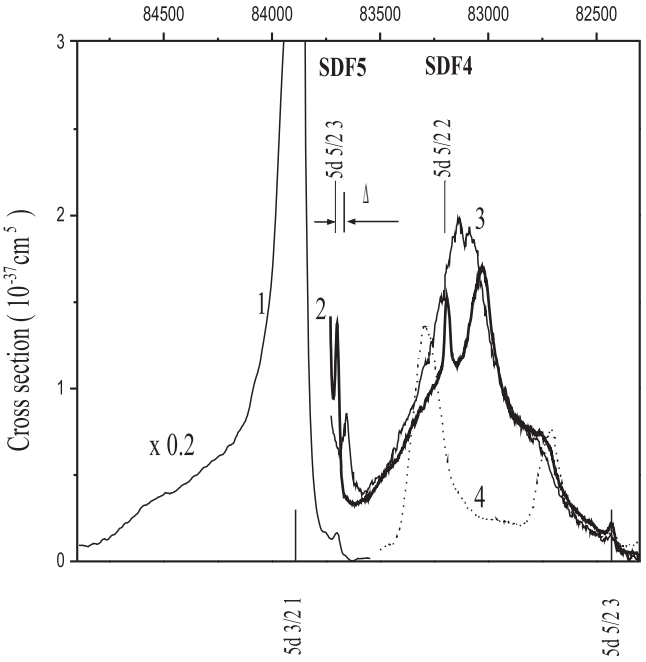

FIG. 4. Absorption cross section near the Xe $5d[3/2]_1$ resonance. Mixtures: Xe 1 mbar/CF_4 300 mbar (1, multiplied by 0.2), Xe 5 mbar/CF_4 230 mbar (2), Xe 5 mbar/C_2F_6 300 mbar (3), Xe 5 mbar/He 260 mbar (4). The lower sticks indicate energies of the Xe atom levels and the upper sticks indicate energies of the Xe atom levels increased by ν_3 quantum energy. $\Delta = \nu_3(CF_4) - \nu_{10}(C_2F_6) = 30\ cm^{-1}$. The gap between two bands in the spectrum of mixture with He is approximately the same energy as between Xe $5d[5/2]_3$ and Xe $5d[5/2]_2$ states (the latter is not on the plot scale).

of the Xe $5d[1/2]_1$ resonance (Fig. 3) and their appearance near Xe $5d[3/2]_1$ (Fig. 4) is due to the large strength of this resonance (Table I).

The very strong Xe $5d[3/2]_1$ resonance may have a satellite. Indeed, the band labeled SR3 in Fig. 2(b) closely matches with the energy of the Xe $5d[3/2]_1$ SR. The Xe/C_2F_6 mixture spectrum in Fig. 2(b) displays a similar band which is shifted to the red due to the difference in ν_3 and ν_{10} energies. It should be noted, however, that in contrast to the spectrally narrow SDFs, SR3 does not match exactly the asymptotic energy of Xe $5d[3/2]_1 + CF_4$ $(\nu_3 = 1)$ (or C_2F_6 $(\nu_{10} = 1)$) pair. In both mixtures, SR3 is shifted by $\sim 10\ cm^{-1}$ to the red, while the parent resonance band is graded to the blue (Fig. 4(a)). A tentative explanation of this shift is an interaction of the resonance dipole with the dielectric continuum which also causes the broadening on the red wing on the Xe $5d[3/2]_1$ resonance (Fig. 4).

The broad band centered at $\sim 83\,100\ cm^{-1}$ in Fig. 4 is related to the Xe $5d[5/2]_3$ state. The high intensity of this band in comparison with C1–C3 in Fig. 3 is likely due to the proximity to the strong Xe $5d[3/2]_1$ resonance. It should be noted that the energy separation between the $83\,100\ cm^{-1}$ band and a broad shoulder on the blue side of the Xe $5d[3/2]_1$ resonance is close to the ν_3-quantum energy. The shoulder may be due to the

$$Xe(5p^6)..CF_4(\nu_3 = 0) + h\nu \rightarrow Xe(5d[5/2]_3)..CF_4(\nu_3 = 1)$$

transitions at small impact parameters for which the upper and lower potentials are not parallel (in contrast to the spec-

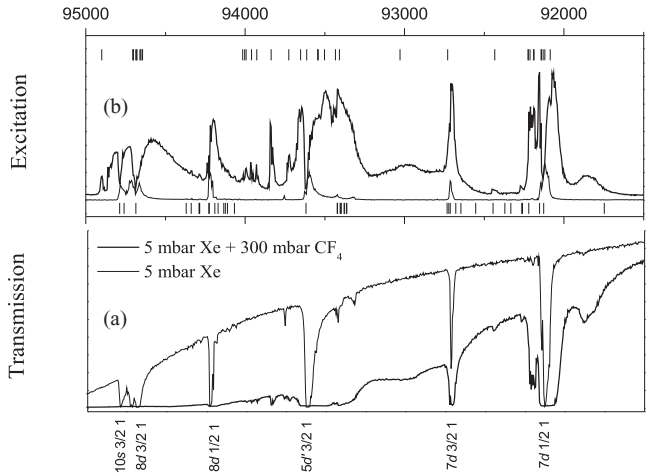

FIG. 5. Transmission (a) and luminescence excitation (b) spectra of Xe and Xe/CF_4 mixture. The lower sticks indicate Xe levels, the upper sticks are the Xe levels displaced by the energy of CF_4 ν_3 quantum.

trally narrow Xe $5d[5/2]_3$ SDF corresponding to a transition between nearly parallel potentials).

D. High-lying states of Xe atom in the λ < 110 nm region

In our previous work,[5] we discussed Xe/CF_4 spectra in the 88 000–91 500 region covering the Xe $8s[3/2]_1$ and Xe $6d[3/2]_1$ resonances. Figure 5 shows an overview of transmission (a) and luminescence excitation (b) spectra further to the blue. The entrance window of the solar blind PMT is made of Mg_2F. The transmission threshold of this material is at ~88 000 cm^{-1} (λ ~114 nm). Therefore, the signal in the excitation spectrum in Fig. 5(b) is due to emission from lower lying resonance states populated collisionally. An alternative mechanism is associative ionization,

$$Xe^{**} + Xe \rightarrow Xe_2^+ + e^-,$$

(threshold energy for this process is 90 150 cm^{-1} (Ref. 25)) followed by ion-electron recombination or dissociative attachment,

$$Xe_2^+ + e^- \rightarrow Xe^* + Xe,$$

in subsequent ion-electron encounters. This process predominantly populates Xe 6*p* and Xe 5*d* states[26] and collisions transfer population to the lowest Xe $6s[3/2]_1$ resonance state.

In mixtures with CF_4, the luminescence signal is stronger than in pure Xe (Fig. 5(b)). This enhancement may be in part due to a more complete population transfer to lower lying states which decay radiatively in the λ>114 nm region, where the PMT is sensitive. Another contribution may be the recombination process $Xe^* + Xe + CF_4 \rightarrow Xe_2^* + CF_4$. The Xe_2^* dimers decay at λ ~175 nm where the sensitivity of the solar blind PMT is likely higher than at shorter wavelengths.

As can be seen from Fig. 5(a), CF_4 itself absorbs Vac UV radiation in this region and the cross section increases with photon energy. This absorption indicates that acceptor states for an intermolecular energy transfer,

$$Xe^{**} + CF_4 \rightarrow Xe + CF_4^*,$$

are available. In collisions with He, the intermolecular energy transfer is excluded and population from Xe** states may only be transferred to the lowest excited Xe 6*s* states. Experiments showed that for the same pressures, luminescence signals from Xe/CF_4 and Xe/He are comparable. It implies that the probability of intermolecular transfer in $Xe^{**} + CF_4$ collisions is small in comparison with relaxation to lower lying states.

Spectra in Fig. 5 display numerous SDFs along with the pressure-broadened resonance transitions. Satellites of Xe 4*f* and Xe 8*s* states appear near the Xe $7d[1/2]_1$ resonance. A striking example of the SDF effect is seen on the blue side of the strong Xe $5d'[3/2]_1$ resonance. These spectral regions are shown in detail with high resolution in Figs. 6 and 7.

Figure 6(a) presents satellites of dipole-forbidden Xe $8s[3/2]_2$ and Xe $4f[5/2]_2$ states (SDF6 and SDF7) and a satellite of the Xe $8s[3/2]_1$ resonance state (SR5) all near the Xe $7d[1/2]_1$ resonance. The SDF7 is a first order effect because the parent state is coupled optically with Xe $7d[1/2]_1$. In contrast to the spectrally broad Xe $6s[3/2]_1$ SR (SR1 in Fig. 2),

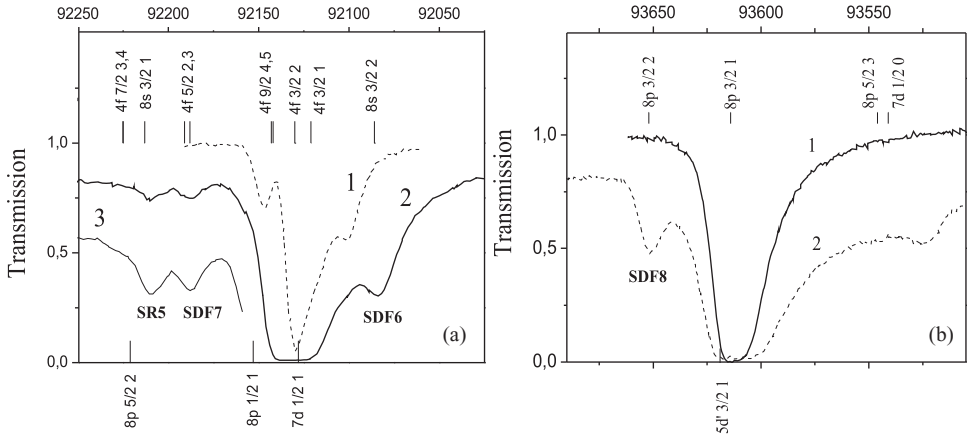

FIG. 6. (a) Transmission spectra near the Xe $7d[1/2]_1$ resonance: 3 mbar Xe (1), 1.3 mbar Xe/60 mbar CF_4 (2), 3 mbar Xe/130 mbar CF_4 (3). (b) Transmission spectra near the Xe $5d'$ $[3/2]_1$ resonance: 2 mbar Xe (1), 2 mbar Xe/15 mbar CF_4 (2). Absorption cross section at the maximum of the Xe $8p[3/2]_2$ SDF is ~5 × 10^{-36} cm^5.

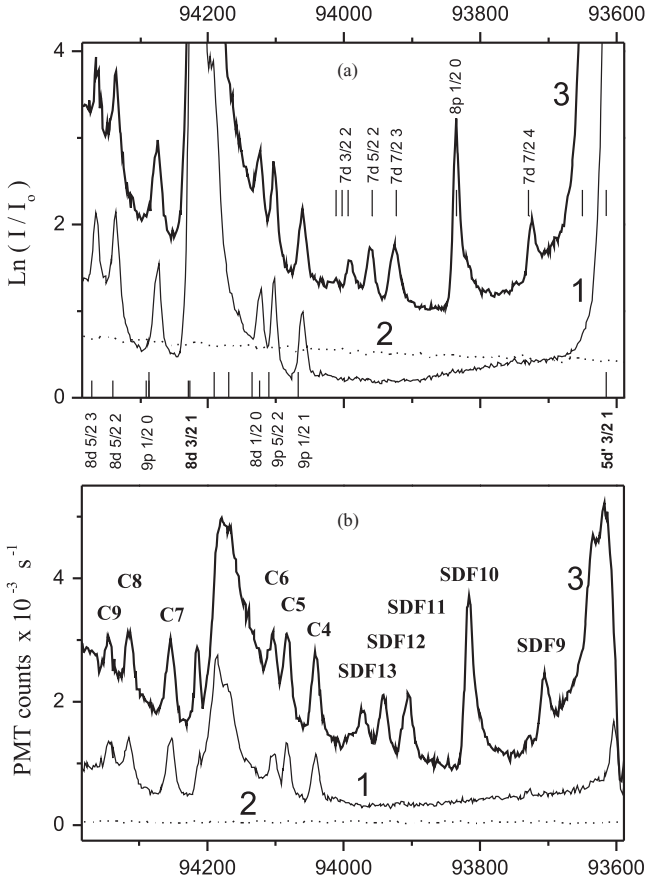

FIG. 7. Absorption (a) and luminescence excitation (b) spectra of Xe 35 mbar (1), CF_4 70 mbar (2), and Xe 35 mbar + CF_4 70 mbar (3). Undispersed luminescence was recorded by a solar blind PMT. The lower set of sticks shows energies of Xe atom levels and the upper set of sticks shows the energies of lower lying Xe levels displaced by the ν_3 quantum energy.

SR5 is a narrow band which matches the asymptotic energy of the collisional pair. As noted in Sec. I, SR of the lowest resonance states correspond to transitions at small impact parameter and they differ from SDF in terms of the intensity borrowing mechanisms. SR5 is likely a second order effect in electric field mixing induced by the CF_4 vibrational dipole similar to SDF6 and other SDFs with parent states not directly coupled with the resonance states.

Figure 6(b) displays the Xe $8p[3/2]_2$ SDF (SDF8) near the Xe $5d'[3/2]_1$ resonance. SDF8 is very strong with an absorption cross section at maximum of $\sigma \sim 5 \times 10^{-36}$ cm^5 and can be seen for partial pressures of Xe and CF_4 of only ~1 mbar. Several weaker SDFs in the region further to the blue from the Xe $5d'[3/2]_1$ resonance are shown in Fig. 7. The satellite of Xe $8p[1/2]_0$ (SDF10) is stronger than the Xe $7d$ SDFs (SF9, SF11–SF13) because its parent state is directly coupled with the Xe $5d'[3/2]_1$ resonance. However, the difference in intensity is only a factor of 3–5 and the Xe $7d$ SDFs are readily seen for the same experimental conditions. In particular, the spectrum displays a satellite of Xe $7d[7/2]_4$ (SDF9). This state may be coupled with the resonance states only in the fourth order of perturbative description of electric field induced mixing (a satellite of the lower lying Xe $6d[7/2]_4$ state has also been observed[5]). As shown above for the Xe $6p$ satellites, at least qualitatively the intensities of these bands can be related to the strengths of transitions to the Xe $6s'$ $[1/2]_1$ and Xe $5d[3/2]_1$ resonance states. Transition strengths between high lying Xe states are not known to date (some preliminary calculations have recently been performed[27]).

The spectral region in Fig. 7 is ~4000 cm^{-1} below the Xe atom ionization threshold, IP(Xe) = 97 873 cm^{-1} (102.17 nm). In principle, interaction of transient dipoles may couple the Xe(DF) + CF_4 ($\nu_3 = 1$) states with optically accessible Xe(IC) + CF_4 ($\nu_3 = 0$) states in the ionization continuum (IC). Although the transitions to IC are weaker than to bound resonance states, this coupling mechanism may contribute to the optical dipole moment of SDF. Interestingly, if the energy gap between a given Xe(DF) state and the ionization threshold is less than the ν_3 quantum energy, the Xe(DF) + CF_4 ($\nu_3 = 1$) state would lie in the ionization continuum and the Xe($IC \leftrightarrow DF$) and CF_4 ($\nu_3 = 0 \leftrightarrow \nu_3 = 1$) transitions would be in an exact resonance.

Another interesting question concerns the photoionization of Xe–CF_4 collisional pairs. As seen from Fig. 5, the luminescence excitation spectrum of mixtures with CF_4 display a continuum in the region on the blue side of the Xe $7d[3/2]_1$ resonance at 107.86 nm. This continuum may be due to associative photoionization,

$$\mathrm{Xe} + \mathrm{CF_4} + h\nu \rightarrow (\mathrm{XeCF_4})^+ + e,$$

followed by dissociative attachment,

$$(\mathrm{XeCF_4})^+ + e \rightarrow \mathrm{Xe}^{**} + \mathrm{CF_4},$$

in subsequent ion-electron encounters. To our knowledge, the threshold energy for this process is not known to date.

Finally, yet another observation should be mentioned. To enhance the intensity of SDFs on the background of the continuous CF_4 absorption, the spectrum 3 in Fig. 7 was recorded at a high Xe pressure and a low partial pressure of CF_4. Spectra of pure Xe (1) and CF_4 (2) are also shown for comparison. As can be seen, the spectrum of pure Xe shows several narrow bands labeled C4–C9. These transitions are induced by collisions with Xe and the energies are close to Xe(DF) + Xe (G) asymptotic energies. Collisions with CF_4 and He only weakly affect intensities and shapes of these bands. It is likely that C4–C9 are due long range interaction of the Xe(DF) + Xe (G) states with states in the Xe_2 ionization continuum. To our knowledge, the Xe spectrum in this region is poorly known. More detailed spectroscopic and theoretical studies appear of interest.

E. Spectroscopy of Xe/C_2F_6 mixtures

Like CF_4, the C_2F_6 molecule has no electron affinity. Its IR spectrum displays a very intense and narrow band corresponding to the ν_{10} mode ($\nu_{10} = 1251$ cm^{-1}), and two weaker bands corresponding to ν_5 (1117 cm^{-1}) and ν_6 (714 cm^{-1}) modes.[28] The ν_{10}:ν_5:ν_3 intensity ratio is approximately 10:3:1.

C_2F_6 is transparent in the $\lambda > 120$ nm region and mixtures containing ~1 bar of this gas can be studied. Similar to CF_4, C_2F_6 efficiently transfers population between excited states of the Xe atom while the nonradiative quenching,

$$\mathrm{Xe}^* + \mathrm{C_2F_6} \rightarrow \mathrm{Xe}(G) + \mathrm{C_2F_5} + \mathrm{F\ (or\ other\ products)},$$

is weak or absent. The quantum yields of Vac UV luminescence following excitation of Xe/CF_4 and Xe/C_2F_6 mixtures in the $\lambda > 120$ nm region are nearly the same.

The shapes of pressure-broadened resonance transitions and their satellites in Xe/C_2F_6 and Xe/CF_4 mixtures are similar, as in particular, was demonstrated above for satellites of resonance Xe $6s[3/2]_1$ and Kr $5s[3/2]_1$ transitions (Fig. 2(c)). The difference in vibrational quanta energies $\Delta = \nu_3(CF_4) - \nu_{10}(C_2F_6) = 30$ cm^{-1} is hardly seen for these spectrally broad satellites. In contrast, for the spectrally narrow satellites, the shift is well resolved. Examples are shown in Figs. 2(d) and 4.

Experiments with Xe/C_2F_6 mixtures conducted in the course of the present study were less extensive in comparison with Xe/CF_4 because of the strong absorption in the spectrally rich $\lambda < 120$ nm region. These experiments were mainly aimed to confirm the main findings for Xe/CF_4. It should be noted that like CF_4 and C_2F_6, more complex perfluorocarbons (C_3F_8, C_4F_{10}) have a similar intense and spectrally narrow absorption band in the IR region.[28] This band is related to the stretch of the C–F bond and is close to 1300 cm^{-1} for all C_nF_{2n+2} molecules. Strong absorption of the polyatomic molecules in the Vac UV region is an obstacle for studies of collision induced effects in spectra of mixtures with Xe. However, systematic studies with a more extended set of C_nF_{2n+2} gases may be conducted for Hg or other atoms for which transitions to high lying states or the ionization continuum are in the region where C_nF_{2n+2} gases are transparent.

F. Vibrational satellites in two-photon LIF spectra

The Xe n$p[1/2]_0$, n$p[3/2]_2$, and n$p[5/2]_2$ states are coupled with the ground Xe $5p^6$ state by two-photon transitions. Similar to one-photon resonances, transitions to two-photon resonance states (TPRS) may have satellites corresponding to the process,

$$\mathrm{Xe}(G) + \mathrm{CF_4}(\nu_3 = 0) + 2h\nu \rightarrow \mathrm{Xe(TPRS)} + \mathrm{CF_4}\ (\nu_3 = 1)$$

Furthermore, electric field induced mixing of two-photon resonance and two-photon forbidden states may cause satellites of two-photon forbidden transitions.

In the course of the present study, test experiments with two-photon excitation of mixtures of Xe with CF_4 and C_2F_6 were conducted. The fundamental frequency of a Lambda Physik dye laser pumped by a Lambda Physik excimer laser was doubled by a BBO-I crystal to obtain UV photons in the region of 40 000 cm^{-1}. Gas mixtures were contained in a metal cell mounted on the entrance slit port of a 0.5 m vacuum monochromator (Minuteman). Laser induced luminescence in the Vac UV region was monitored via a side-on window by a solar-blind photomultiplier. The two-photon absorption cross sections is small and in comparison with the one-photon experiments, much higher partial pressures were required to observe weak bands. Typical mixtures consisted of ~1 bar of Xe and ~3 bar of CF_4 or C_2F_6. The emission spectra of these high-pressure mixtures display a broad Xe_2* band centered at $\lambda \sim 175$ nm. At low pressure, the 147 nm resonance band of the Xe atom was seen, but the red-shifted satellite transition

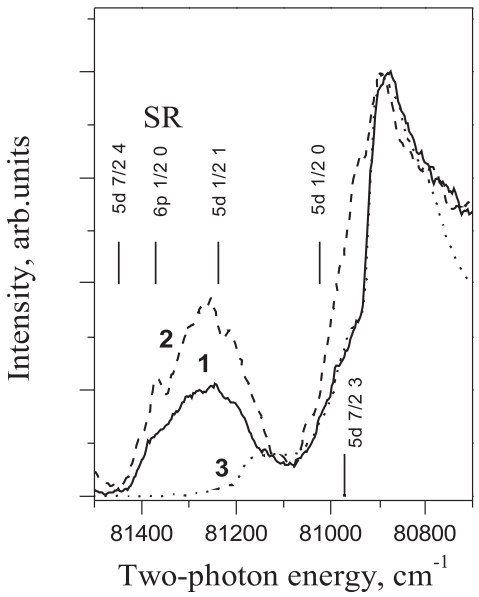

FIG. 8. Two-photon Vac UV luminescence excitation spectra: Xe 1 bar/CF_4 2.5 bar (1), Xe 1 bar/C_2F_6 2.5 bar (2), Xe 1 bar/Ar 2.5 bar (3). Luminescence was monitored at $\lambda \sim 175$ nm (maximum of Xe_2 emission band). The lower stick indicates the Xe $5d[7/2]_3$ state energy, the upper sticks indicate energies of lower lying states shifted by ν_3 quantum energy of CF_4.

to the vibrationally excited ground state,

$$\mathrm{Xe}(6s[3/2]_1) + \mathrm{CF_4}(\nu_3 = 0) \rightarrow \mathrm{Xe}(^1\mathrm{S}_0) + \mathrm{CF_4}(\nu_3 = 1) + h\nu,$$

was not found in these spectra.

Figure 8 shows excitation spectra on the blue wing of the Xe $6p[1/2]_0$ two-photon resonance (one photon spectrum in this region is shown in Fig. 4). The resonance band is saturated at these high pressures and is not shown in Fig. 8. The band around 80 800 cm^{-1} is seen in all mixtures and is likely related to the two-photon forbidden Xe $5d[7/2]_3$ state. In contrast, the band around 81 300 cm^{-1} is not seen in mixture with Ar. This band is close to the energy of the Xe $6p[1/2]_0$ two-photon resonance state increased by one vibrational quantum energy of CF_4 (C_2F_6), and therefore, it is attributed to its vibrational satellite.

In the course of the present work, test LIF experiments in the region of the higher lying Xe $6p'$ and Xe $7p$ states were conducted as well. This region is especially interesting because numerous satellites of the Xe $7p$ and Xe $6d$ states were observed in one-photon spectra.[5] Unfortunately, because of the small cross section for Xe $7p$ and Xe $6p'$ two-photon resonances and a decrease of the frequency-doubling efficiency, the LIF signal was too weak. Studies of two-photon excitation of jet-cooled Xe-CF_4 and Xe-C_2F_6 vdW molecules using sensitive REMPI detection might give interesting results.

IV. CONCLUSION

Spectroscopic studies of Xe/CF_4 mixtures have shown that a strong IR active mode of a molecule may induce a large manifold of satellite transitions in the spectra of atom-molecule collision pairs. When the energy gap between Xe(R) and Xe(DF) is close to the ν_3 quantum energy and Xe($R \leftrightarrow DF$) is an allowed optical transition, the Xe(DF) + CF_4 ($\nu_3 = 1$) and Xe(R) + CF_4 ($\nu_3 = 0$) states are mixed by the

dipole-dipole interaction, and SDF acquires a very large strength. It is striking that some satellites are readily seen both in absorption and in luminescence excitation spectra for partial pressures of Xe and CF_4 in the gas cell around only 1mbar.

Spectra also display numerous SDFs for which the parent states are not optically coupled with the resonance states. These SDFs may be explained as a higher order effect of electronic state mixing induced by the CF_4 ($\nu_3 = 0 \leftrightarrow \nu_3 = 1$) transient dipole.[5] This mechanism seems not to be applicable for the spectrally broad satellites of the lowest resonance transitions in Xe and Kr atoms. The resonance states may be coupled with each other via intermediate np-states. In particular, Kr $5s[3/2]_1$ and Kr $5s'[1/2]_1$ SRs are nearly identical in shape and intensity, although the parent state of the latter SR is a factor of two closer to Kr $5p$ states which may act as intermediate. These bands are likely due to inelastic scattering of the Rydberg electron on the CF_4 molecule causing its vibrational excitation. This question requires further studies.

Owing to large ν_3 (CF_4) quantum energy, the population of $\nu_3 = 1$ level at room temperature is negligible which prevents observation of

$$\mathrm{Xe}(G) + \mathrm{CF_4}\ (\nu_3 = 1) + h\nu \rightarrow \mathrm{Xe}(DF) + \mathrm{CF_4}\ (\nu_3 = 0)$$

transitions corresponding to a vibrational deactivation of CF_4. These transitions would be strongly enhanced by mixing with a $\mathrm{Xe}(R) + \mathrm{CF_4}$ ($\nu_3 = 1$) resonance state, if the Xe(R) state is below Xe(DF) and the energy gap is $\sim\nu_3$ (CF_4). For example, this condition is met for the Xe $8s[3/2]_1$ resonance state and Xe $8p$ forbidden states (Fig. 1). In principle, the

$$\mathrm{A}(G) + \mathrm{M}(\nu_{\mathrm{IR}} = 1) + h\nu \rightarrow \mathrm{A}(DF) + \mathrm{M}(\nu_{\mathrm{IR}} = 0)$$

transition enhanced by proximity to a $\mathrm{A}(R) + \mathrm{M}(\nu_{\mathrm{IR}} = 0)$ resonance may be used for optical cooling. Assuming that the gas mixture is in a cavity of a transparent matrix, and $\mathrm{M}(\nu_{\mathrm{IR}} = 0) \rightarrow \mathrm{M}(\nu_{\mathrm{IR}} = 1)$ and $\mathrm{A}(DF) \rightarrow \mathrm{A}(R)$ processes are due to energy transfer from/to matrix, the cooling effect would take place, if ν_{IR} is larger than the energy gap between A(DF) and A(R). Essential requirements are radiative decay of A(R) in the transparency window of the matrix, stability of A(R) in respect of collisional quenching, and relatively small ν_{IR} energy to ensure significant population at room temperature.

As noted in Sec. I, simultaneous optical excitation of two ground state atoms has been observed before.[8,9] In context to the present studies in the Vac UV region, we mention that the process

$$\mathrm{Xe}(G) + \mathrm{Am}(G) + h\nu \rightarrow \mathrm{Xe}(DF) + \mathrm{Am}(R),$$

where Am is an alkali atom, may be observed when the Am (n$s \leftrightarrow$ np) resonance transition and Xe($R \leftrightarrow DF$) transition are close in energy, although continuous absorption to alkali ionization continuum would be a complication for such studies. Another interesting example of such a process in the Vac UV region is

$$\mathrm{H}(1s) + \mathrm{Li}(2s) + h\nu \rightarrow \mathrm{H}(2s) + \mathrm{Li}(2p).$$

The Li ($2s \leftrightarrow 2p$) energy is $\sim$330 cm^{-1} less than that of H ($2s \leftrightarrow 3p$) and, the transition to H ($2s$) + Li ($2p$) is shifted by the same amount from the H ($1s \rightarrow 3p$) Lβ resonance. Because of the large abundance of Li and H, this process is of astrophysical interest and may also find applications for diagnostics of H rich plasmas employing a Li beam method (Ref. 29 and references therein). In a broader sense, $\mathrm{A}(G) + \mathrm{B}(G) + h\nu \rightarrow \mathrm{A}(DF) + \mathrm{B}(R)$ transitions enhanced by an accidental proximity of $\mathrm{A}(DF \leftrightarrow R)$ and $\mathrm{B}(G \leftrightarrow R)$ transitions may likely be found in spectra of other binary systems ranging from the deep IR to inner shell excitations in the x-ray region. Such processes may be of interest for light emitting technology to increase efficiency of broadband optical excitation of luminophores, optical cooling, monitoring transient species, and concentrations of their precursors and other applications.

ACKNOWLEDGMENTS

The results reported in this paper have been recorded at BESSY during several beamtimes in 2006–2009. We are grateful to the BESSY staff and especially to Dr. G. Reichardt. V.A.A. acknowledges financial support from the Deutsche Forschungsgemeinschaft via Sfb 450 and via an individual grant in 2007 and also from the Russian-German beamline project at BESSY.

[1] M. C. Castex, J. Chem. Phys. **66**, 3854 (1977).
[2] D. E. Freeman, K. Yoshino, and Y. Tanaka, J. Chem. Phys. **67**, 3462 (1977).
[3] V. A. Alekseev, Opt. Spectrosc. **96**, 492 (2004).
[4] V. A. Alekseev, AIP Conf. Proc. **1058**, 163 (2008).
[5] V. A. Alekseev and N. Schwentner, Chem. Phys. Lett. **436**, 327 (2007).
[6] V. A. Alekseev and N. Schwentner, Chem. Phys. Lett. **463**, 47 (2008).
[7] V. A. Alekseev, J. Grosser, O. Hoffman, and F. Rebentrost, J. Chem. Phys. **129**, 201102 (2008).
[8] J. C. White, G. A. Zdasiuk, J. F. Young, and S. E. Harris, Opt. Lett. **4**, 137 (1979).
[9] R. Hotop and K. Niemax, J. Phys. B **13**, L93 (1980).
[10] L. I. Gudzenko and S. I. Yakovlenko, Sov. Phys. JETP **35**, 877 (1972).
[11] S. Geltman, Phys. Rev. A **35**, 3775 (1987), and references therein.
[12] K. S. Smirnov, M. A. Nikolskaya, and A. A. Tsyganenko, Opt. Spectrosc. **62**, 743 (1987).
[13] N. N. Filippov, J.-P. Bouanich, C. Boulet, M. V. Tonkov, R. Le Doucen, and F. Thibault, J. Chem. Phys. **106**, 206 (1997).
[14] O. Oehler, D. A. Smith, and K. Dressler, J. Chem. Phys. **66**, 2097 (1977).
[15] P. L. Kunsch and K. Dressler, J. Chem. Phys. **68**, 2550 (1978).
[16] C. Crepin and A. Tramer, J. Chem. Phys. **107**, 2205 (1997).
[17] C. E. Moore, "Atomic energy levels," *National Bureau of Standards Circular No. 467* (U.S. GPO, Washington, DC, 1958), Vol. III.
[18] G. Reichardt, J. Bahrdt, J.-S. Schmidt, W. Gudat, A. Ehresmann, R. Muller-Albrecht, H. Molter, H. Schmoranzer, M. Martins, N. Schwentner, and S. Sasaki, Nucl. Instr. Meth. A **467–468**, 462 (2001).
[19] V. A. Alekseev, N. Schwentner, D. Cappelletti, F. Pirani, O. Alekseeva, M. Lednev, A. Zagrebin, and M. Bartolomei, AIP Conf. Proc. **1058**, 166 (2008).
[20] G. L. Gutsev, Chem. Phys. **163**, 59 (1992).
[21] R. H. Lipson and R. W. Field, J. Chem. Phys. **110**, 10653 (1999) and references therein.
[22] D. A. Dixon, J. Phys. Chem. **92**, 86 (1988).
[23] M. Aymar and M. Coulombe, At. Data Nucl. Data Tables **21**, 537 (1978).
[24] *NIST Computational Chemistry Comparison and Benchmark Database*, NIST Standard Reference Database Number 101, Release 15a, April 2010, edited by D. Russell Johnson III, http://cccbdb.nist.gov/
[25] X. K. Huo, D. M. Mao, Y. J. Shi, S. S. Dimov, and R. H. Lipson, J. Chem. Phys. **109**, 3944 (1998).
[26] R. H. Lipson, X. K. Hu, J. B. A. Mitchell, and C. Froese-Fischer, J. Phys.: Conf. Ser. **4**, 216 (2005).
[27] A. V. Loginov, unpublished private communication (2007).
[28] P. M. Chu, F. R. Guenther, G. C. Rhoderick, and W. J. Lafferty, "Quantitative infrared database," in *NIST Chemistry WebBook, NIST Standard Reference Database Number 69*, edited by P. J. Linstrom and W. G. Mallard (National Institute of Standards and Technology, Gaithersburg, MD, 2005), p. 20899.
[29] G. Anda, G. Petravich, S. Zoletnik, and S. Bato, Fusion Eng. Des. **74**, 715 (2005).